metals

MDPI

Article

Study on Microstructure and Properties of a New Warm-Stamped Niobium-Alloyed Steel

Peng Tian [1], Wen Liang [1], Zhennan Cui [1], Guoming Zhu [1,*], Yonglin Kang [1,*], Baoshun Li [1], Li Lin [2] and Rendong Liu [2]

[1] School of Material Science and Engineering, University of Science and Technology Beijing, Beijing 100083, China
[2] Ansteel Technology Center, Anshan 114009, China
* Correspondence: zhuguoming@ustb.edu.cn (G.Z.); kangylin@ustb.edu.cn (Y.K.); Tel.: +86-10-6233-2335 (G.Z. & Y.K.); Fax: +86-10-6233-2983 (G.Z. & Y.K.)

Received: 21 May 2019; Accepted: 3 July 2019; Published: 8 July 2019

Abstract: The warm stamping technology is a promising technology to meet the needs of car weight reduction and energy conservation. In order to compare with the mechanical properties of the traditional hot-stamped boron-alloyed steel 22MnB5, a new warm-stamped niobium-alloyed steel 22Mn3SiNb was designed and tested. The optimal heating parameters for warm forming process were explored through mechanical tests, and the process of their microstructure evolution was investigated by scanning electron microscope (SEM), transmission electron microscope (TEM) and X-ray diffraction (XRD), etc. The experimental results indicate that the optimal heating parameters for the niobium-alloyed steel 22Mn3SiNb are a heating temperature of 800 °C and a soaking time of 5 min. Compared to the hot-stamped boron-alloyed steel 22MnB5 under their respective optimal heating parameters, the properties and microstructure characteristics of 22Mn3SiNb are greatly improved, and nearly no decarburized layer is found on the surface of the niobium-alloyed steel 22Mn3SiNb. In addition, the addition of Nb produces the effects of grain refinement and precipitation strengthening due to the introduction of plenty of nano-precipitated particles and dislocations. In the end, it can be predicted that the new warm-stamped niobium-alloyed steel will replace the conventional hot-stamped boron-alloyed steel.

Keywords: warm stamping technology; boron-alloyed steel; hot-stamped steel; niobium-alloyed

1. Introduction

The rapid development of the automobile industry aggravates the increasing consumption of energy and serious pollution of the environment, lightening of the automobile is one of the most paramount measures to reduce fuel consumption and exhaust emissions [1,2]. With the increase in the use of advanced high-strength steels in body-in-white, such as dual-phase (DP) steel, transformation induced plasticity (TRIP) steel, quenching and partitioning (Q&P) steel and twinning induced plasticity (TWIP) steel, significant achievements have been made in the lightening of automobiles. Up to now, the proportion of high-strength steel in the body of the car has exceeded 60% [3,4]. What is worth to be sure is that under the same structural strength conditions, the use of hot-stamped steel can greatly reduce the weight of the parts and produce less deformation during the collision, which can effectively protect the safety of passengers.

For the hot-tamped boron-alloyed steel 22MnB5, a host of experts have conducted in-depth reports. Admittedly, the conventional hot-stamped steel 22MnB5 has a tensile strength of 1500 MPa, nevertheless, its total elongation is not over 7% and it is formidable to improve it. Generally, the traditional hot-stamped steel 22MnB5 has the following disadvantages [5–10].

(1) The austenitizing temperature is too high, which leads to severe oxidation of the slab surface. In order to solve this problem, the Si-Al anti-oxidation coating is employed, but it greatly increases the cost of hot-stamped steel.

(2) The cooling rate for hot-stamped steel 22MnB5 needs to be large enough to obtain a complete martensitic microstructure. However, high cooling rates can result in cracks or residual stresses in the component.

According to the latest research, the warm stamping technology of the medium manganese steel could replace the traditional hot-stamped steel 22MnB5 to a certain extend in the future. In order to distinguish from the traditional hot stamping technology, the lower heating temperature processing technology is called the warm stamping technology. The advantages of warm stamping technology of the medium manganese steel can be summarized as the following three points [11–17].

(1) For automotive structural components, lower heating temperature produces less oxidation and decarbonization, which will generate finer grain size. The substructure of lath martensite also can improve the strength and plasticity of steel. In addition, lower heating temperature decreases energy usage, improves service life of high-temperature structural components, and reduces the investment cost of production line.

(2) The excellent hardenability of the medium manganese steel increases the uniformity of mechanical properties of different parts of the components, so that the warm stamping technology can produce large-sized automobile components.

(3) Encouragingly, the demand of lower cooling rate can reduce the cost of stamping mold.

However, although the warm forming technology of medium manganese steel has such a great advantage, the medium manganese steel has a high alloy cost because the manganese content is as high as 5% or more [13–15]. In recent years, the addition of Nb, Ti, and Nb + Ti to 22MnB5 has achieved good microstructure and performance at a lower cooling rate after hot-stamped, but the austenitizing temperature is still at a high temperature, around 950 °C [18–20]. In this work, a new warm-stamped niobium-alloyed steel 22Mn3SiNb was designed and tested in order to avoid the disadvantages of medium manganese steel and hot-stamped steel. Through comparison with the traditional hot-stamped boron-alloyed steel 22MnB5, the optimum parameters of warm forming process, microstructure evolution, and properties analysis were investigated.

2. Material and Experimental Procedures

2.1. Material

The materials investigated in this work were the niobium-alloyed steel 22Mn3SiNb and the boron-alloyed steel 22MnB5, the chemical composition of that is given in Table 1. The two steels were prepared as 50 kg ingots using vacuum induction melting (VIM), and hot-rolled to 2 mm in thickness after holding 2 h at 1200 °C. Then cut to sheets of 280 mm (length) × 70 mm (width) × 2 mm (thickness) while ensuring that the length direction is parallel to the rolling direction. The processes of warm/hot stamping were conducted in the die with the cooling paths, and the steel sheets were transferred to the die after different heating temperatures and soaking times to obtain the uniform microstructure, then formed and simultaneously quenched at a cooling rate over 20 °C/s in the die. The sheets were kept between the dies for 10 s to obtain U-channel parts with high geometrical accuracy. Figure 1 is the mold of warm/hot stamping.

Table 1. Chemical composition of the investigated steels (mass fraction, %).

Steels	C	Mn	Si	Nb	P	S	Cr	Mo	B
22Mn3SiNb	0.20	3.58	1.58	0.039	0.008	0.005	-	-	-
22MnB5	0.204	1.26	0.256	-	0.005	0.0016	0.281	0.145	0.004

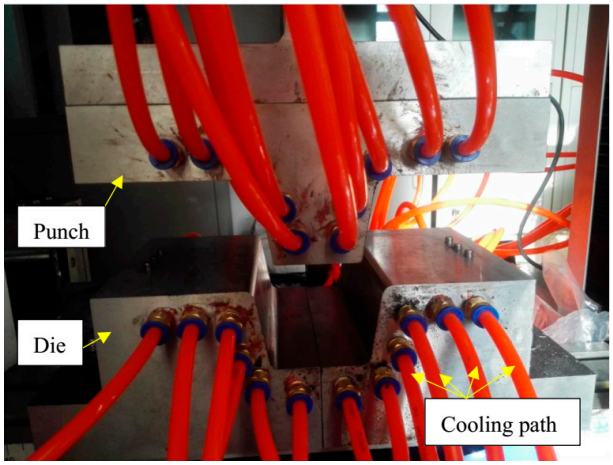

Figure 1. The mold of warm/hot stamping.

2.2. Experimental Procedures

Experiment 1: continuous cooling transformation (CCT) curve. The samples were heated to 1000 °C at the heating rate of 10 °C/s by a thermal dilatometer DIL805A (Baehr Thermonalysis, Ochtrup, Germany) and fully austenitized by holding for 300 s to obtain a uniform temperature field, then cooled to room temperature at cooling rates of 1, 5, 10, 20, 30, 50 °C/s by N_2, respectively. Finally, the microstructures at different cooling rates were obtained through the microscope. CCT curve and Martensitic starting transformation temperature (Ms) were drawn and found out, respectively, by using the tangent method according to the cooling curves.

Experiment 2: mechanical performance tests. The shape and dimensions of the specimens for tensile tests are shown in Figure 2, and the tensile tests at room temperature were performed on the tensile testing machine MTS810 (MTS, Minneapolis, MN, USA) with a tensile speed of 2 mm/min according to the standard of GB/T 228.1-2010. In addition, Kahn tear tests were conducted on the electronic universal testing machine WDW-200D (Sankun Co., Yangzhou, China) to examine fracture toughness after quenching the testing steels according to the standard of ASTM B187-2013. The characteristics of Kahn tear tests are: small test size, simple operation, sharp fracture, easy to produce cracks, ability to accurately measure crack propagation, and obtaining fracture surface for observation and analysis. The shape and dimensions of the specimens for tensile tests are shown in Figure 3, and the loading rate is 2 mm/min. Furthermore, the Vickers hardness of each sample is also measured.

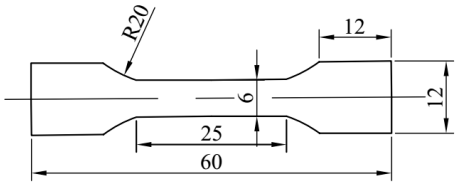

Figure 2. Shape and dimensions of the specimens for tensile tests (mm).

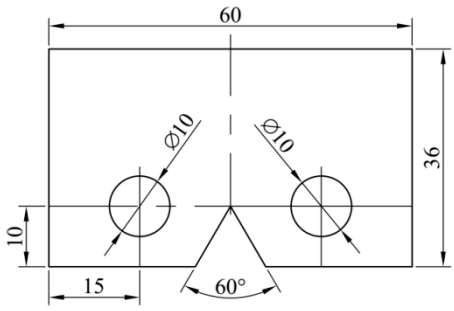

Figure 3. Shape and dimensions of the specimens for Kahn tear tests (mm).

Experiment 3: microstructure characterization. Samples for metallic phase analysis were cut from the quenched steel sheets, the optical microscope (OM) (Eclipse LV150, Ruich Allway, Beijing, China) and scanning electron microscope (SEM) (Quanta FEG450, FEI corporation, Hillsboro, OR, USA) were used to observe the microstructure of hot-rolling and warm/hot-stamping after grinding, polishing, and erosion with 4% Nital solution. In addition, the fracture surfaces were inspected using the scanning electron microscope. Moreover, the samples after grinding and mechanically polishing were soaked in a saturated picric acid solution at 70 °C and for 3 min, then wiped clean with the alcohol and the austenite grain size was observed under OM. The martensite lath and precipitated particles were examined by the transmission electron microscope (TEM) (Hitachi H-8100, Hitachi, Tokyo, Japan) at 200 kV, samples were obtained by carbon extraction replication on Cu-grids, and the 400 μm foils were mechanically thinned to about 50 μm, and were fabricated by twin-jet electrolytic polishing in a mixed solution (95 mL alcohol + 5 mL perchloric acid) at about −30 °C by the twin-jet electropolisher (DJ2000, Dedong Technology Co., Beijing, China). X-ray diffraction (XRD) (MXP21VAHF, Mac, Tokyo, Japan) analysis for the samples being grinded and polished was carried out to investigate the fraction of martensite phase and determine whether retained austenite exists, its technical indicators include Cu Kα radiation, lynxeye-xe detector (Bruke co., Karlsruhe, Germany), and pdf dataset PDF2-2004.

3. Results and Discussion

3.1. Determination of Mechanical Properties and Process Parameters of Experimental Steel

3.1.1. Measurement of Phase Transition Point and CCT Curve

The microstructures of the 22Mn3SiNb steel after continuous conversion at the different cooling rates are shown in Figure 4, and all the microstructures are martensite through metallographic observation. On the one hand, the higher content of Mn and Nb elements significantly increases the hardenability, consequently the matrix structure can be fully converted to martensite at slightly slower cooling rates. On the other hand, the addition Mn and Nb elements improves the stability of austenite, resulting in an increase in the incubation period of austenite phase transformation to other phases, and only martensitic transformation occurs at different cooling rates. So, it can be said that, even if the 22Mn3SiNb steel is cooled to room temperature by air after heating to the full austenitizing temperature, the matrix remains martensite.

Figure 5 manifests the CCT curve of two investigated steels plotted by thermal expansion data. It can be seen from Figure 5a that the austenite region of the niobium-alloyed steel 22Mn3SiNb is increasingly broadly stable, and it transforms to martensite after quenching. In addition, since it possesses a strong hardenability, it can be considered that there is no need for a water-cooled mold in the warm stamping process, and higher strength and better plasticity can be obtained. It can be found from Figure 5b [21] that the whole martensite structure can be obtained when the cooling rate reaches 20 °C/s or more for 22MnB5 and the Ms of it is 80 °C higher than that of 22Mn3SiNb, so a water-cooled mold is necessary for 22MnB5.

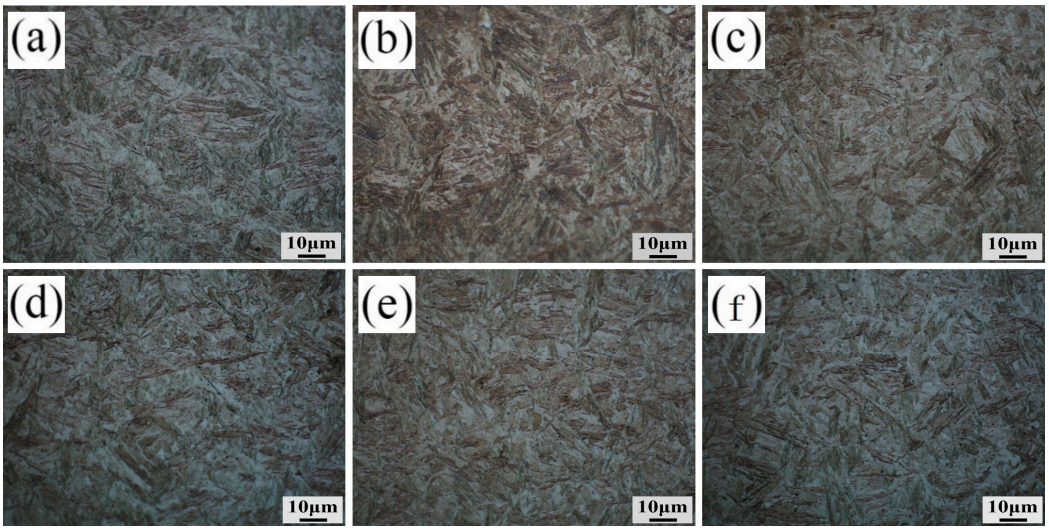

Figure 4. The microstructures of the 22Mn3SiNb steel at the different cooling rates. (**a**) 1 °C/s, (**b**) 5 °C/s, (**c**) 10 °C/s, (**d**) 20 °C/s, (**e**) 30 °C/s, (**f**) 50 °C/s.

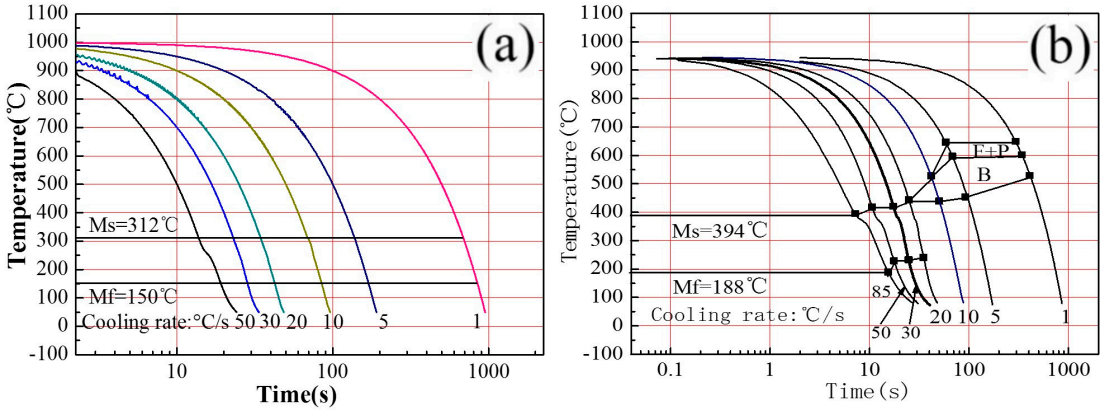

Figure 5. CCT curves of two investigated steels. (**a**) 22Mn3SiNb, (**b**) 22MnB5.

3.1.2. Optimum Forming Process Parameters

The mechanical properties of the two experimental steels were analyzed before warm/hot stamping for comparison. The tensile stress-strain curves of the samples before the warm/hot stamping of the two samples are shown in Figure 6. Table 2 shows the mechanical properties before stamping. Section 3.1.1 gives the basis which concludes that the microstructure of the 22Mn3SiNb steel can form entirely martensite even in the air-cooled state, and it eventually enters the rank of ultra-high strength steel because its tensile strength is close to 1600 MPa, as shown as in Figure 6 and Table 2.

Then, the best heating process parameters of the two experimental steels were studied. The heating process was heated to a certain temperature for a certain period of time and then quenched.

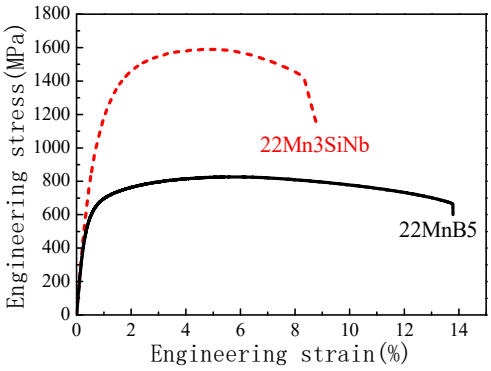

Figure 6. Engineering stress-strain curves of samples before warm/hot stamping.

Table 2. Mechanical properties before warm/hot stamping.

Steel	Rp0.2 (MPa)	Rm (MPa)	A (%)
22MnB5	587	826	13.78
22Mn3SiNb	1014	1589	8.8

Figure 7 describes the mechanical properties of the two experimental steels after being heated for 3 min and 5 min. It can be seen that the tensile strength, yield strength, and elongation of 22Mn3SiNb are about 1400 MPa, 1250 MPa, and 9.5%, respectively, when the heating temperature is 500 °C. However, when the heating temperature increases from 550 °C to 750 °C, the tensile strength and yield strength of the 22Mn3SiNb steel basically decrease with increasing temperature, and the elongation increases with the heating temperature. When the heating temperature is increased from 850 °C to 950 °C, the tensile strength and yield strength of the 22Mn3SiNb steel are about 1650 MPa and 1200 MPa, and the elongation is approximately 11% and 12% when the soaking time is 3 min and 5 min. It is worth noting that the 22Mn3SiNb steel holds the tensile strength of 1590 MPa, yield strength of 989 MPa, elongation of 12.2%, and strength-ductility balance of 19.4 GPa% when the heating temperature is 800 °C and the soaking time is 5 min, which means that the heating temperature of the 22Mn3SiNb steel is about 800 °C. Under the same conditions for 22MnB5, when the holding time is constant and the heating temperature is lower than 750 °C, the yield strength is below 650 MPa, the tensile strength is below 850 MPa. As the heating temperature rises from 750 °C, the yield strength and tensile strength show a significant upward trend, and the elongation decreases rapidly. When the heating temperature exceeds 850 °C and rises to 950 °C, the holding time is 3 min. The yield strength and tensile strength decreased first and then increased, and the elongation trend was reversed. When the holding time is 5 min, as the heating temperature increases from 850 °C to 950 °C, the yield strength, tensile strength, and elongation both decrease first and then increase. In summary, the optimum heating process parameters of 22MnB5 are heating temperature of 950 °C and holding time of 5 min. The best performance parameters are tensile strength around 1600 MPa, yield strength around 1150 MPa, and elongation between 7% and 8%.

The mechanical properties of the two experimental steels were compared after obtaining the best heating process parameters. Table 3 shows the mechanical properties of the two experimental steels under the optimal heating process. According to the analysis summarized in Table 3, when the heating temperature is 800 °C and the heating time is 5 min, the tensile strength of 22Mn3SiNb is 1590 MPa, and the elongation is 12.2%. It is particularly worth mentioning that the mechanical properties of 22Mn3SiNb are much better than that of 22MnB5 and its heating temperature is 150 °C lower. Therefore, it can be inferred that the warm stamping process can significantly reduce the scale and decarburization compared with the hot stamping process, while improving efficiency and energy saving.

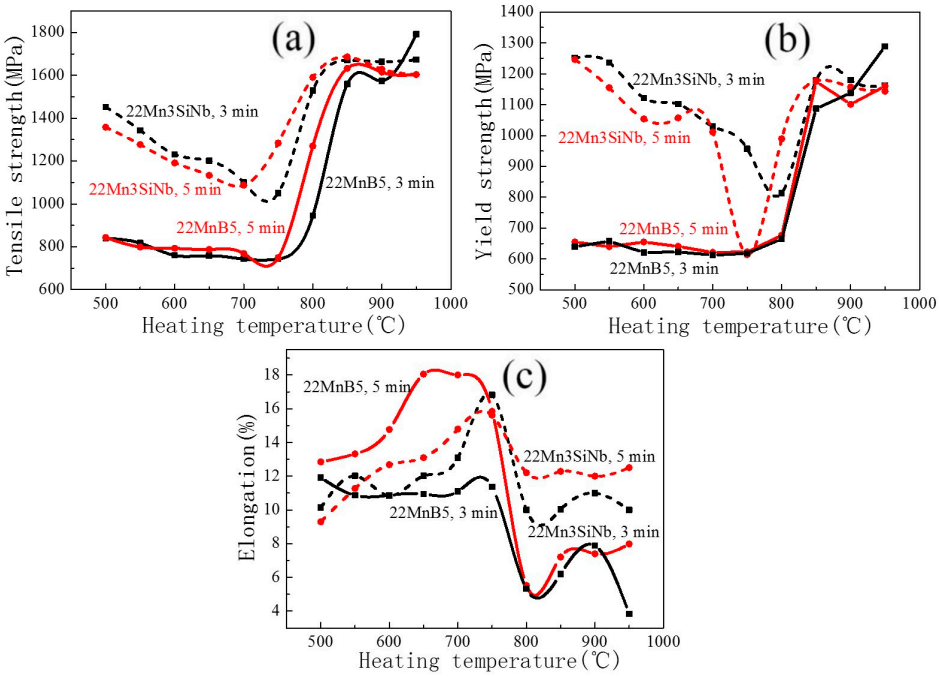

Figure 7. Mechanical properties of the two experimental steels after being heated for 3 min and 5 min, respectively. (**a**) tensile strength, (**b**) yield strength, (**c**) elongation.

Table 3. Mechanical properties of two investigated steels after warm/hot stamping.

Steels	Soaking Time (min)	Heating Temperature (°C)	Rm (MPa)	Rp0.2 (MPa)	A (%)	Yield Ratio	Rm × A (GPa·%)
22Mn3SiNb	5	800	1590	989	12.2	0.62	19.4
22MnB5	5	950	1603	1160	7.98	0.72	12.8

In order to further compare the mechanical properties of the two experimental steels, the hardness test and the fracture toughness test were separately performed. The trend of hardness variation of two investigated steels after being heated at different soaking times is shown in Figure 8. When the soaking time is 3 min, as shown in Figure 8a, the hardness of the 22Mn3SiNb steel is about 350–400 HV when the heating temperature is lower than 800 °C, but it exceeds 450 HV when the heating temperature exceeds 850 °C. Similarly, at the same soaking time, the hardness of the 22MnB5 steel is about 250–320 HV when the heating temperature is lower than 850 °C, but it increases with the increasing of the heating temperature, which is consistent with the trend of corresponding tensile strength. It can be seen from Figure 8b that the Vickers hardness values of two investigated steels are basically maintained at 450–500 HV when the heating temperature exceeds 800 °C and the soaking time is 5 min, which meets the performance requirement of the automotive parts.

The Kahn tear test is employed to measure the fracture toughness by its measurement results, such as unit initiation energy (UIE), unit propagation energy (UPE) and tear strength (TS). TS can be expressed as Equation (1).

$$TS = \frac{P}{A} + \frac{MC}{I} = \frac{4P}{bt}(\text{MPa}), \quad (1)$$

where P is the maximum applied load, A is the effective area of the sample, M is the moment of inertia, C is the turning radius, I is the rotational inertia, b is the minimum width of the sample notch, t is the minimum thickness of the sample.

UIE and UPE can be expressed as Equations (2) and (3).

$$UIE = \frac{s_1}{A} = \frac{s_1}{bt}(\text{N/m}), \quad (2)$$

$$UPE = \frac{s_2}{A} = \frac{s_2}{bt}(\mathrm{N/m}), \tag{3}$$

where s_1 is the energy required for crack formation, s_2 is the energy consumed after crack expansion.

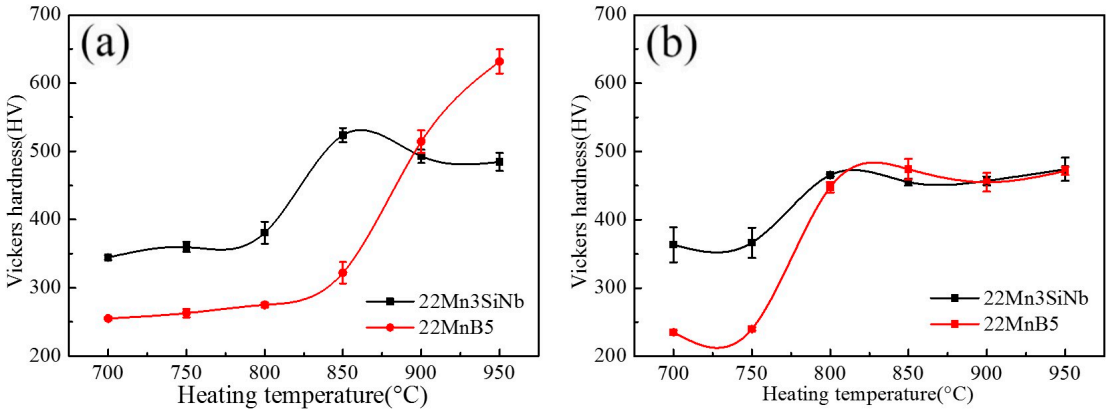

Figure 8. Hardness of two investigated steels after being heated at different soaking times. (**a**) 3 min, (**b**) 5 min.

Figure 9 is the force-displacement curves of the Kahn tear test after quenching on the 22Mn3SiNb steel at a heating temperature of 800 °C for a holding time of 5 min, and the 22MnB5 steel at a heating temperature of 950 °C for a holding time of 5 min. According to Figure 10 and other related data, TS, UIE, UPE, s_1 and s_2 can be obtained, and the results are presented in Table 4. It can be found that compared to the conventional hot-stamped steel 22MnB5, the TS, UIE and UPE of the niobium-alloyed steel 22Mn3SiNb increases by 31%, 173%, and 244%, respectively. Consequently, it can be demonstrated that the 22Mn3SiNb steel has better fracture toughness because it requires and consumes more energy.

As a whole, when the heating parameters are the heating temperature of 800 °C and the soaking time of 5 min, the niobium-alloyed steel 22Mn3SiNb reaches the level of ultra-high strength steel with an excellent elongation. Compared to the traditional hot-stamped steel 22MnB5, which the heating temperature is 950 °C and the soaking time is 5 min, the warm-stamped niobium-alloyed steel is 150 °C lower than it, which greatly saves energy and reduces the scale. Furthermore, the mechanical properties of the warm-stamped steel 22Mn3SiNb is superior to that of the traditional hot-stamped steel 22MnB5, and it is foreseeable that it is likely to replace the hot-stamped steel in the future, achieving the goal of further vehicle weight reduction and energy conservation.

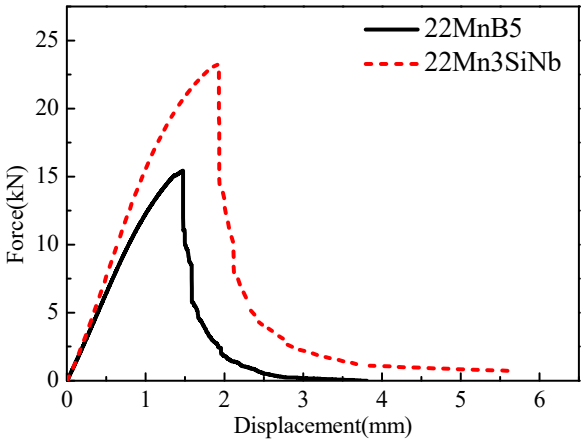

Figure 9. The force-displacement curves of the Kahn tear test.

Table 4. Tear properties of two investigated steels.

Steels	TS (MPa)	UIE (kN/m)	s_1 (J)	UPE (kN/m)	s_2 (J)
22Mn3SiNb	1762	495	25.7	275	14.3
22MnB5	1341	181	9.4	80	4.2

3.2. Study on Strengthening Mechanism of a Warm-Stamped Niobium-Alloyed Steel

3.2.1. Microstructure Characteristics

Figure 10 presents the SEM micrographs of hot-rolled steels. It can be observed that the microstructure of the 22Mn3SiNb steel is martensite and a small amount of feathered bainite, which is due to the higher hardenability, whereas the microstructure of the 22MnB5 steel is ferrite and pearlite. In order to observe the decarburization on the surface of the test steel, the microstructures of the 22Mn3SiNb steel and the 22MnB5 steel after being quenched at 800 °C and 950 °C for 5 min, respectively, were subjected to metallographic analysis. As shown in Figure 11, it can be seen that the decarburized layer is approximately 40 μm of the 22MnB5 steel, which consists of ferrite and pearlite. However, it is worth nothing that nearly no decarburized layer is found on the surface of the 22Mn3SiNb steel.

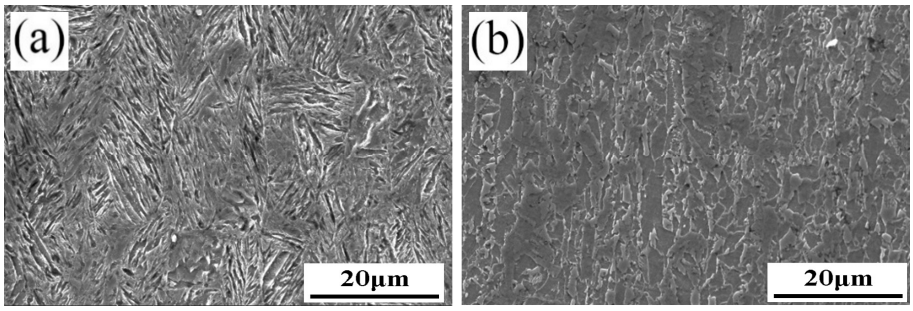

Figure 10. SEM micrographs of hot-rolled steels. (**a**) 22Mn3SiNb, (**b**) 22MnB5.

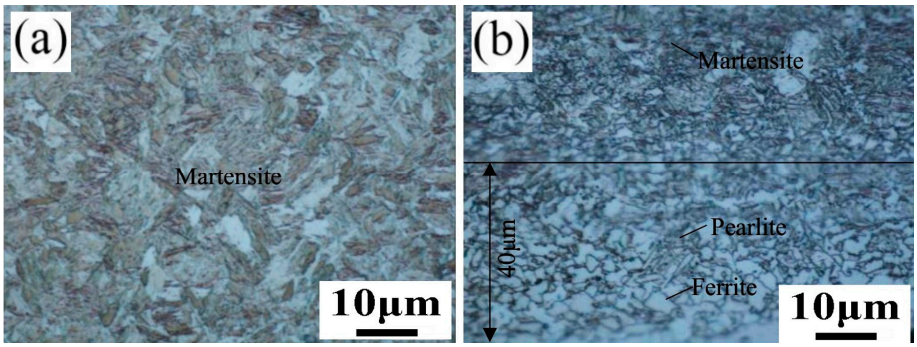

Figure 11. The decarburized layers of two investigated steels after stamping and quenching. (**a**) 22Mn3SiNb, 800 °C–5 min, (**b**) 22MnB5, 950 °C–5 min.

Figure 12 are the SEM micrographs of two investigated steels after heating for 5 min. As presented in Figure 12a, when the heating temperature is 750 °C and the soaking time is 5 min, the microstructures of the 22Mn3SiNb steel are composed of the feathered bainite and considerable martensite. When the heating temperature is increased to 800 °C, as shown in Figure 12b, the microstructure of the 22Mn3SiNb steel has been completely transformed into an intensely fine martensite structure, which explained the high tensile strength of about 1590 MPa. Certainly, the abrupt changes have occurred in macro mechanical properties, such as tensile strength and elongation. Compared with the 22Mn3SiNb steel, a typical ferrite and martensite dual phase microstructure can be easily found in

Figure 12c for the 22MnB5 steel. However, a fully martensite structure can be presented in Figure 12d, which means the heating temperature is about 900 °C.

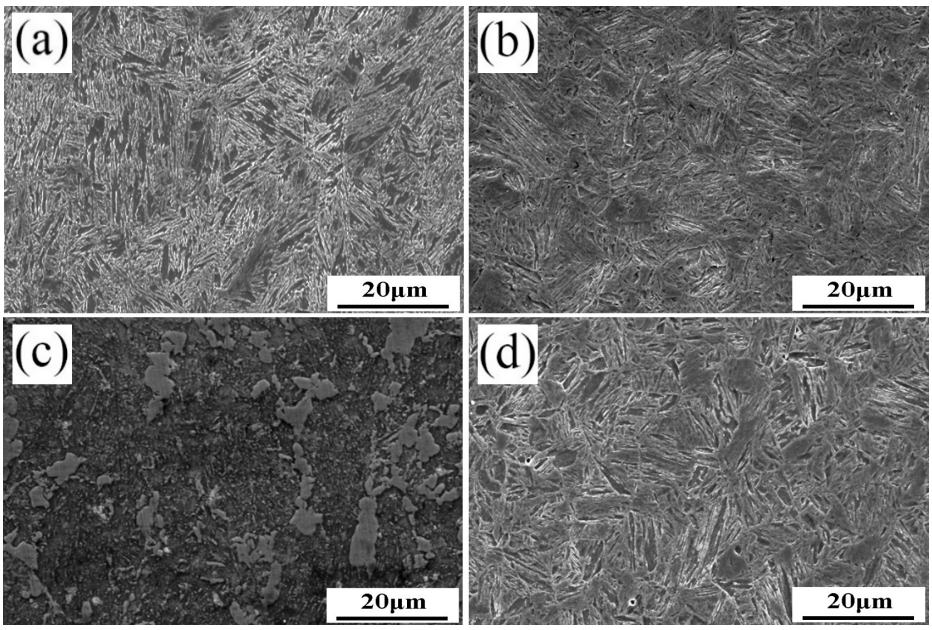

Figure 12. SEM micrographs of two investigated steels after heating for 5 min. (**a**) 22Mn3SiNb, 750 °C, (**b**) 22Mn3SiNb, 800 °C, (**c**) 22MnB5, 800 °C, (**d**) 22MnB5, 900 °C.

Figure 13 shows XRD patterns of the 22Mn3SiNb steel at 800 °C with 5 min and the 22MnB5 steel at 950 °C with 5 min, it shows that there are three phases of martensite, retained austenite and other phases such as aluminum oxide. Quantification with Rietveld analysis found 98.8% martensite, 1.1% retained austenite, and 0.1% other phases for 22Mn3SiNb, while found 98.2% martensite, 1.4%, and 0.4% other phases for 22MnB5. Comparing the two XRD peak-shaped curves, the retained austenite in 22MnB5 is more obvious and it includes three peaks of (111)γ, (200)γ, and (311)γ. In order to understand the detailed microstructure, TEM was carried out to observe the martensite lath, as presented in Figure 14. It can be observed that the microstructure of both test steels consists of lath martensite and there are a large number of dislocations inside or at the boundary of martensite. The martensitic lath widths of the warm-stamped 22Mn3SiNb steel and the hot-stamped 22MnB5 steel were measured by Image-tool software, and were 184 nm and 374 nm, respectively. This shows that the lath martensite width of the warm-stamped 22Mn3SiNb steel is significantly smaller than that of the hot-stamped 22MnB5 steel.

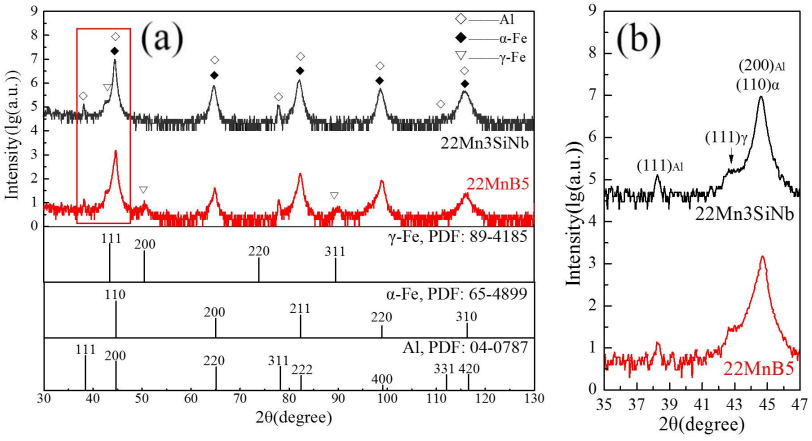

Figure 13. XRD patterns of two investigated steels. (**a**) 30 ≤ 2θ ≤ 130, (**b**) 35 ≤ 2θ ≤ 47.

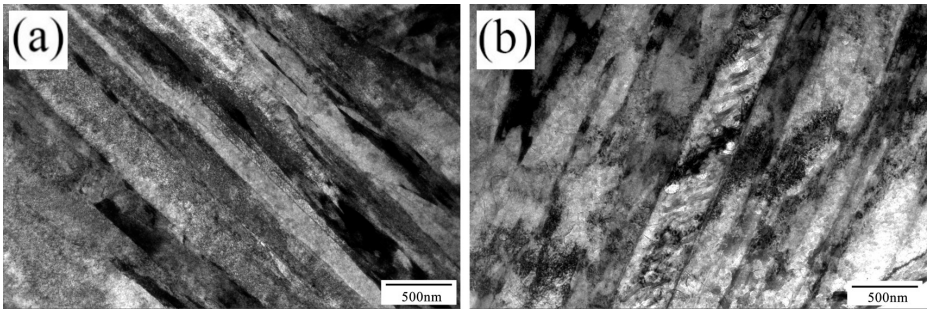

Figure 14. TEM micrographs of lath martensite of two investigated steels after heating for 5 min. (**a**) 22Mn3SiNb, 800 °C, (**b**) 22MnB5, 950 °C.

As shown in Figure 15, in order to analyze the microstructure quantitatively, the prior austenite grain size (PAGS) of two investigated steels after heating for 5 min were determined by linear intercept measurements. 100 prior austenite grains in Figure 15 were randomly measured using Image-tool software, and the PAGS is 6.2 μm and 13.1 μm, respectively. It is evident that the PAGS of the niobium-alloyed steel 22Mn3SiNb is smaller than that of the hot-stamped steel 22MnB5.

The PAGS of the 22Mn3SiNb steel is relatively tiny, the reason is that on the one hand, the hardenability of it is greatly improved due to the presence of Mn element, and on the other hand, as a result of the alloying element Nb, which has the effect of grain refinement and precipitation strengthening, the austenite grain growth is prevented during heating [22,23].

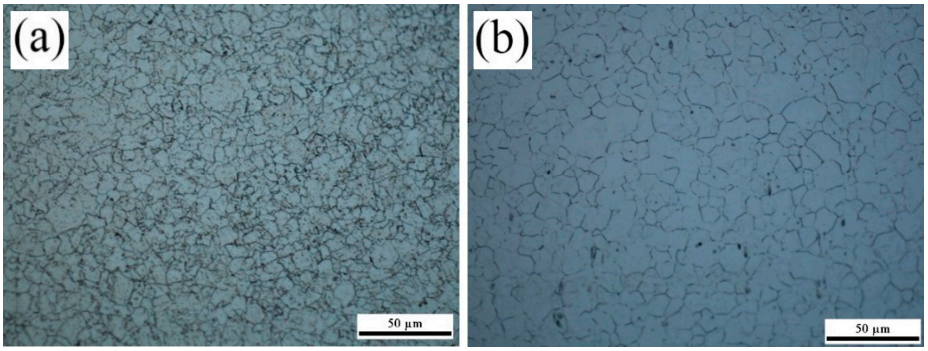

Figure 15. OM images of prior austenite grain of two investigated steels after heating for 5 min. (**a**) 22Mn3SiNb, 800 °C; (**b**) 22MnB5, 950 °C.

3.2.2. Effect of Precipitates on the Microstructure

In general, grain refinement and precipitation strengthening in strengthening mechanisms are considered to increase strength without loss of material toughness and formability [24]. Figure 16 presents the TEM images of two investigated steels. Plenty of dislocations and precipitates [19] are exist in the martensite lath for 22Mn3SiNb and only dislocations for 22MnB5, and they are interweaved each other to hinder the slipping of possible slip systems. However, the size of cementite is relatively small. Lin et al. [19] thought this is mainly due to the fact that the niobium element is first precipitated in combination with carbon and nitrogen elements, which reduces the carbon and nitrogen content. At the same time, the dislocations in the martensite laths have a dislocation strengthening effect on the martensitic matrix.

Figure 17 is the TEM images of the precipitation and energy dispersive spectrometer (EDS) of the 22Mn3SiNb steel. It can be seen that the nano-precipitated particles exist in the interior of the martensite lath, and the great majority of these particles are spherical in shape to keep the low interfacial energy [25]. Combined with EDS of the precipitates, it can be concluded that the precipitates is Nb(C, N) in the 22Mn3SiNb steel. Figure 17b shows the results of quantitative analysis with and without

the C element, the comparison shows that C element has a great influence on the quantitative analysis of trace elements for samples prepared by carbon replication. Furthermore, over 200 particles were measured by the area method from the TEM images and the average particles diameter was then obtained. Figure 17d shows that the particles size distribution conforms to normal distribution, the particles size is 5~20 nm, and the average particles diameter is about 8.9 nm. Due to the high hardness of the nano-precipitates, the dislocations can only be moved by the bypass mechanism during the deformation, thus leaving a series of dislocation loops at the precipitated particles, thereby increasing the critical force of the dislocation movement and providing precipitation strengthening effect.

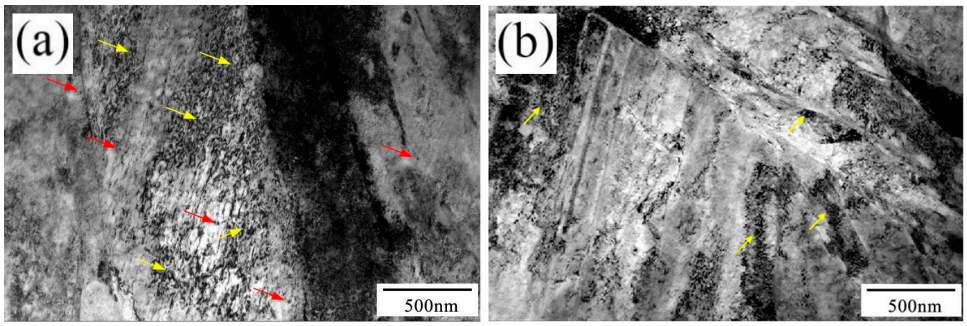

Figure 16. TEM images of two investigated steels. The red arrows represent the Nb(C, N), yellow arrows represent the dislocation. (**a**) 22Mn3SiNb, (**b**) 22MnB5.

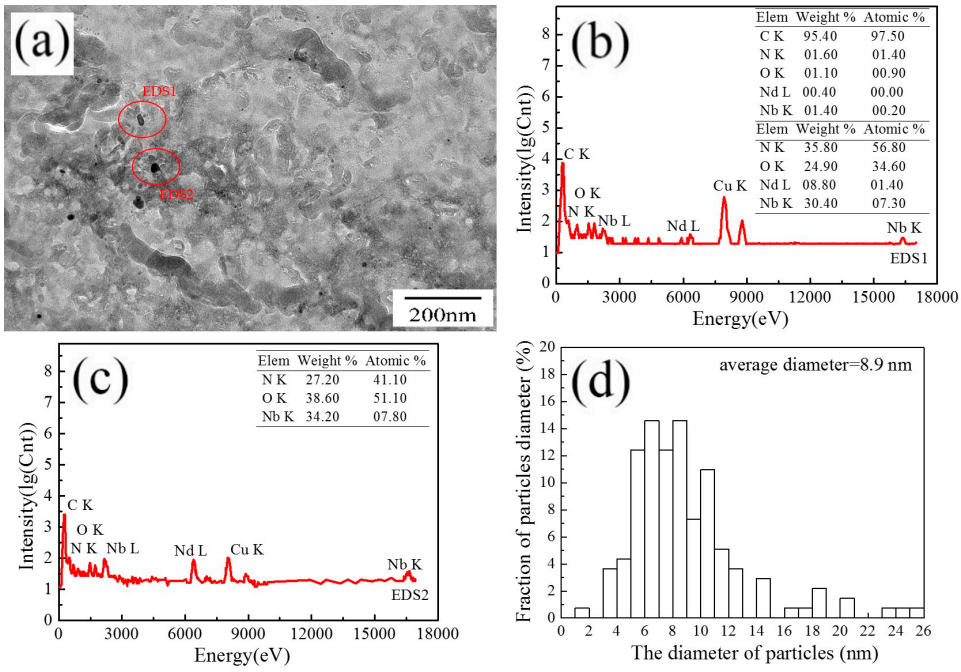

Figure 17. TEM images of the precipitation and EDS of the 22Mn3SiNb steel. (**a**) TEM images of precipitation particles, (**b**,**c**) precipitation particles for EDS, (**d**) size distribution.

3.2.3. Fracture Interfaces

Figure 18 shows the SEM images of the fracture interfaces of two investigated steels. From the Figure 18a, a dimple characteristic with few quasi-cleavage characteristics are observed on the fracture interface of the 22Mn3SiNb steel when the heating temperature is 800 °C and the soaking time is 3 min. Figure 18b shows the typical cleavage surface and tearing ridge characteristics are found on the fracture interface of 22MnB5 at a heating time of 900 °C and a holding time of 3 min. As shown in Figure 18c, obvious dimple characteristics are displayed on the fracture interface of the 22Mn3SiNb

steel at 800 °C for 5 min, and the dimples are deeper and smaller compared with these at 3 min. However, the fracture morphology of the 22MnB5 steel at 950 °C for 5 min is mainly composed of quasi-cleavage characteristics and large and shallow dimples presented in Figure 18d.

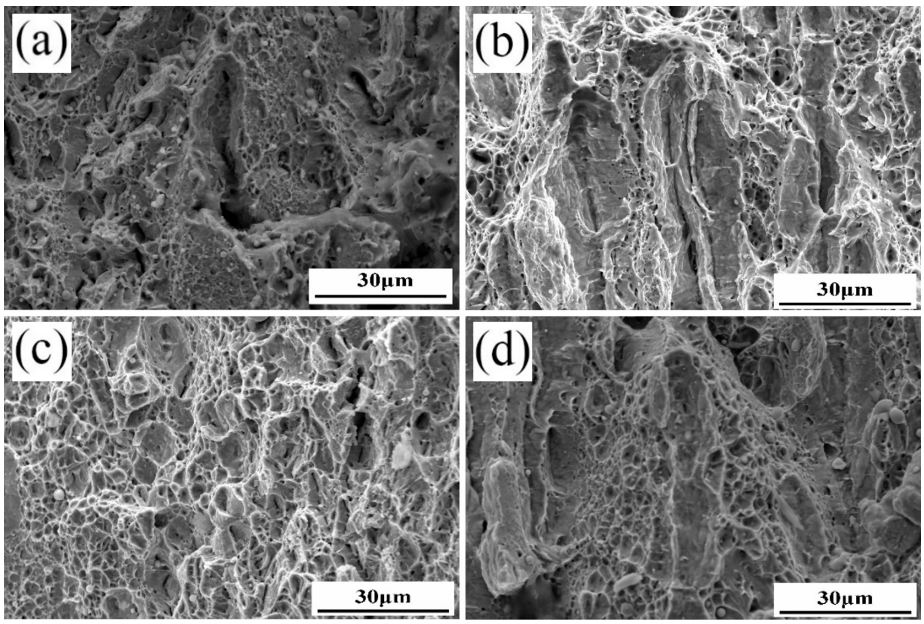

Figure 18. Fracture surfaces of two investigated steels. (**a**) 22Mn3SiNb, 800 °C–3 min, (**b**) 22MnB5, 900 °C–3 min, (**c**) 22Mn3SiNb, 800 °C–5 min, (**d**) 22MnB5, 950 °C–5 min.

3.2.4. Strengthening Mechanism

Ultrafine grain is the core of the development of the third generation high-strength steel, which has become a consensus. After the grain refinement of the steel, dislocations are more difficult to cross grain boundaries, so that the strength and the plasticity of the steel are extremely improved. The niobium-alloyed steel 22Mn3SiNb enjoys excellent comprehensive mechanical properties mainly benefitted from its small martensitic lath widths and more dislocations and precipitated particles. It is worth nothing that its small martensitic lath widths not only enhances the strength of the steel sheet, but also improves the plasticity very well. For each 1% increase in the content of manganese, Ms temperature decreases by approximately 30.4 °C, and the drop of Ms temperature makes the warm forming technology of the niobium-alloyed steel feasible. Simultaneously, the addition of manganese can also increase the hardenability of the steel sheet, and the content of hard phase martensite is higher in the cooled microstructure. In addition, the solid solution strengthening effect produced by the manganese element can enhance the strength of the steel sheet, thereby achieving a favorable combination of formability and strength [26].

It is noteworthy that Nb element was added to the 22Mn3SiNb manganese steel, which produced fine grain strengthening and precipitation strengthening effects. The addition of Nb not only allows the investigated steel to obtain the full martensite structure at a lower cooling rate, but also the precipitates formed with the carbon and nitrogen elements strengthen the matrix. According to the second phase theory of steel [27], dissolved Nb in steel will form precipitated particles with carbon and nitrogen at high temperature, and these precipitated particles will always exist and affect the subsequent transformation of the microstructure. The solubility product of the precipitated phase formed by Nb element in the steel can be expressed by Equation (4) [28].

$$T_{As} = \frac{B}{A - \lg[w(M)\, w(X)]}, \tag{4}$$

where T_{As} is the temperature of solubility, A and B, respectively, is constant for each precipitation, $w(M)$ and $w(X)$ are the mass fraction of precipitated element A and B. The solubility product of the carbides or nitrides of niobium in austenite is illustrated in Figure 19 (formulas from [27]). It is evident that when the heating temperature is 800 °C, Nb is rarely dissolved in austenite, and almost all Nb elements are present in austenite in the form of precipitated particles. It hinders the austenite grain boundary from moving outwards through pinning and increases the driving force required for the grain boundary to move, resulting in a significant obstruction of austenite grain growth.

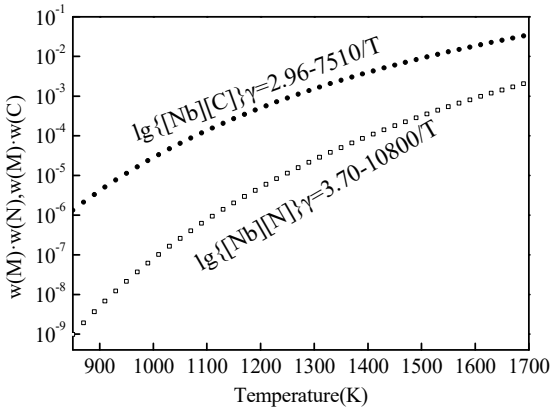

Figure 19. Solubility product of carbide or nitride for Nb in austenite.

For martensitic steels, the strength is determined by the size of the three substructures within the prior austenite grains, which are the martensite lath, block and packet [29–31], as presented in Figure 20. The prior austenite grains can be divided into several martensite packets, which consist of a group of martensite laths with the same habit plane, while the martensite block can be divided into sub-block which consists of some martensitic laths with same orientation and variants. The relation of Kurjumov-Sachs (K-S) crystallographic between the martensite laths and the prior austenite is (111)γ//(011)α, <110>γ//<111>α, and the 24 crystallographic variants (V1–V24) in martensite form four kinds of packet. Furthermore, the microstructure of the niobium-alloyed steel 22Mn3SiNb after warm stamping is affected by the prior austenite grains, and the characteristics of martensite block and packet are hereditary, which meets the Hall-Petch relationship with the yield strength. It should be noted that the size of the martensite lath, as an effective grain size of the martensite structure, is a paramount factor in determining the strength of the martensitic steel [32].

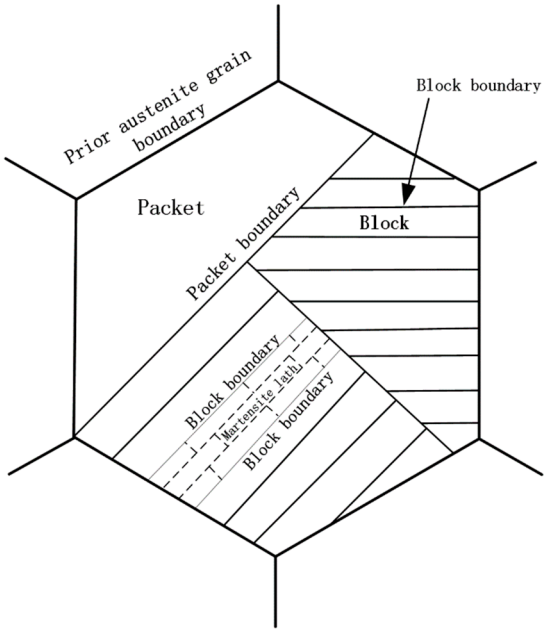

Figure 20. Schematic illustration showing the multi-scale structure of lath martensite.

4. Experimental Verification of the Warm Stamping Niobium-Alloyed Steel

In order to verify the heating process parameters identified in Section 3.2, i.e., the heating temperature is 800 °C and the soaking time is 5 min, the niobium-alloyed steel 22Mn3SiNb was subjected to a warm stamping test on the mold as shown in Figure 1, similarly, the hot stamping parameters of 22MnB5 were at 950 °C and 5 min, and the U-channel parts shown in Figure 21a were finally obtained, the scale on the surface of 22MnB5 is more than that of 22Mn3SiNb. Then six quintessential locations presented in Figure 21b were selected to measure the mechanical properties, and the tensile test specimens were prepared from the coupons to the similar dimensions of the specimen shown in Figure 2. Three mechanical properties are displayed in Figure 22, such as tensile strength, yield strength, and elongation. Figure 22a demonstrates that the niobium-alloyed steel 22Mn3SiNb shows uniform distributions of mechanical properties, the average values of tensile strength, yield strength and elongation are 1602 MPa, 976 MPa and 12.2% respectively. From the Figure 22b, the mechanical properties' stability of 22MnB5 is not as good as that of 22Mn3SiNb, the average values of tensile strength, yield strength and elongation are 1621 MPa, 1138 MPa and 8.5%. By comparing the experimental data, we can see that the uniformity of mechanical properties of 22Mn3SiNb are much better than that of 22MnB5 and its heating temperature is 150 °C lower, at the same time, its performance is better than that of medium manganese steel and its manganese content is significantly reduced [12–14]. As a result, the new warm-stamped niobium-alloyed steel 22Mn3SiNb is promising for automotive structural parts, replacing the hot-stamped boron-alloyed steel 22MnB5 and the warm-stamped medium-Mn steel.

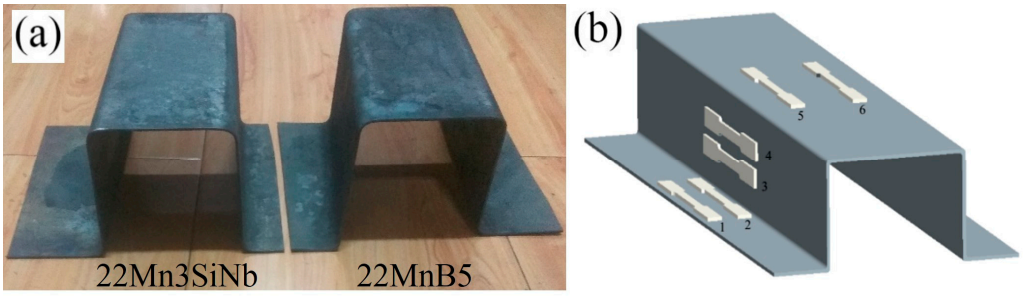

Figure 21. The U-shaped parts and sample location diagram. (**a**) U-channel parts, (**b**) sample location.

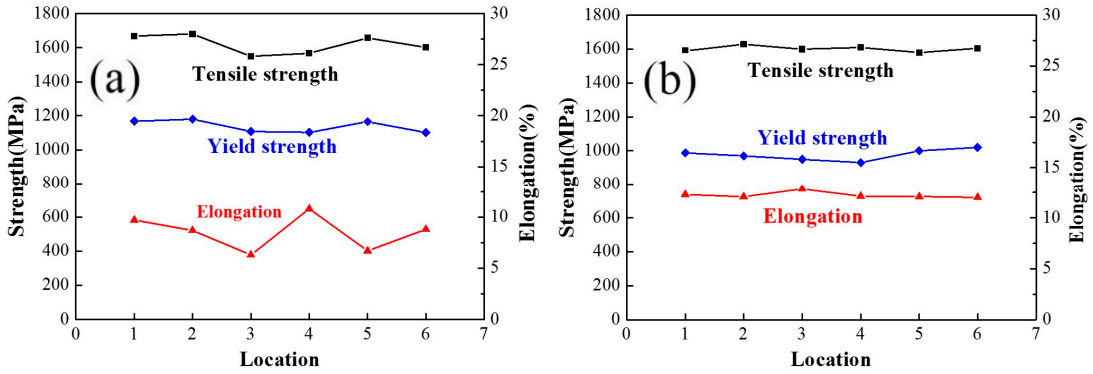

Figure 22. Mechanical properties at six typical locations of the U-shaped parts. (**a**) 22Mn3SiNb, (**b**) 22MnB5.

5. Conclusions

(1) By comparing the CCT curves of 22Mn3SiNb and 22MnB5, the austenite region of the niobium-alloyed steel 22Mn3SiNb is increasingly broadly stable. Due to 22Mn3SiNb's strong hardenability, it can be considered that there is no need for a water-cooled mold in the warm stamping process, but it is necessary for 22MnB5.

(2) The optimal heating parameter for 22Mn3SiNb is a heating temperature of 800 °C and a soaking time of 5 min, and it enjoys the tensile strength of 1590 MPa, the yield strength of 989 MPa, and the elongation of 12.2% under this condition. Furthermore, compared with the hot-stamped steel 22MnB5, it possesses better fracture toughness and its heating temperature is lower than 150 °C.

(3) Compared to the hot-stamped steel 22MnB5, the microstructures of the 22Mn3SiNb steel after warm stamping are finer, such as the prior austenite grain and the martensite. Moreover, nearly no decarburized layer is found on the surface of it, and obvious dimple characteristics are displayed on the fracture interface of it and the dimples are deeper and smaller through the fractography analysis. All these result in better mechanical properties of the 22Mn3SiNb steel.

(4) The addition of Nb in the 22Mn3SiNb steel not only allows it to obtain the martensite structure at a lower cooling rate, but also the precipitates formed with the carbon and nitrogen elements strengthen the matrix. The size of nano-precipitated particles is 5~20 nm and the average particles diameter is about 8.9 nm.

(5) A true warm stamping U-channel part of 22Mn3SiNb and 22MnB5 were performed using the optimal heating parameter. The final part of 22Mn3SiNb shows a more uniformly-distributed mechanical properties than that of 22MnB5. It proves that the warm stamping technology for the new niobium-alloyed is a promising technology to manufacture the high or ultrahigh strength steel, which will replace the hot-stamped boron-alloyed steel 22MnB5 in the near future.

Author Contributions: Conceptualization, G.Z. and Y.K.; methodology, P.T.; software, W.L.; validation, P.T. and W.L.; formal analysis, B.L.; investigation, L.L. and R.L.; resources, W.L. and Z.C.; data curation, P.T.; writing-original draft preparation, P.T., Z.C. and B.L.; writing-review and editing, P.T.; visualization, W.L.; supervision, G.Z.; project administration, G.Z.; funding acquisition, G.Z. and Y.K.

Funding: This research was funded by University of Science and Technology Beijing, grant number FRF-AT-18-009.

Acknowledgments: The authors acknowledge funding from University of Science and Technology Beijing (FRF-AT-18-009).

Conflicts of Interest: The authors declare no conflicts of interest.

References

1. Kang, Y.L. *Theory and Technology of Processing and Forming for Advanced Automobile Steel Sheets*; The Metallurgical Industry Press: Beijing, China, 2009; pp. 509–512.
2. Venezuela, J.; Zhou, Q.; Liu, Q.; Zhang, M.; Atrens, A. Hydrogen trapping in some automotive martensitic advanced high-strength steels. *Adv. Eng. Mater.* **2018**, *20*, 1700468. [CrossRef]
3. Gan, Y.; Li, G.Y.; Ma, M.T. Development of advanced compact steel process and deep working technology for high-strength-ductility auto-parts. *Steel Roll.* **2015**, *32*, 1–12.
4. Li, G.Y.; Ma, M.T.; Zhang, Y.S.; Luo, R. Advanced hot forming treatment AHFT of deep working technology for ultra- high-strength-ductility auto-parts. *Steel Roll.* **2015**, *32*, 1–8.
5. Karbasian, H.; Tekkaya, A.E. A review on hot stamping. *J. Mater. Process. Technol.* **2010**, *210*, 2103–2118. [CrossRef]
6. Takahashi, M.; Nakata, M.; Imai, K.; Kojima, N.; Otsuka, N. Liquid metal embrittlement of hot stamped galvannealed boron steel sheet-effect of heating time on crack formation. *ISIJ Int.* **2017**, *57*, 1094–1101. [CrossRef]
7. Abbasi, M.; Saeed-Akbari, A.; Naderi, M. The effect of strain rate and deformation temperature on the characteristics of isothermally hot compressed boron-alloyed steel. *Mater. Sci. Eng. A* **2012**, *538*, 356–363. [CrossRef]
8. Yogo, Y.; Kurato, N.; Iwata, N. Investigation of Hardness Change for Spot Welded Tailored Blank in Hot Stamping Using CCT and Deformation-CCT Diagrams. *Met. Mater. Trans. A* **2018**, *49*, 2293–2301. [CrossRef]
9. Ikeuchi, K.; Yanagimoto, J. Valuation method for effects of hot stamping process parameters on product properties using hot forming simulator. *J. Mater. Process. Technol.* **2011**, *211*, 1441–1447. [CrossRef]
10. Liu, H.; Lu, X.; Jin, X.; Dong, H.; Shi, J. Enhanced mechanical properties of a hot stamped advanced high-strength steel treated by quenching and partitioning process. *Scr. Mater.* **2011**, *64*, 749–752. [CrossRef]
11. Li, X.D.; Han, S.; Wang, C.Y.; Hu, P.; Dong, H. Research on the warm-hot forming process and its performance evaluation for the third-generation automobile steel. *J. Mech. Eng.* **2017**, *53*, 35–42. [CrossRef]
12. Chang, Y.; Wang, C.; Zhao, K.; Dong, H.; Yan, J. An introduction to medium-Mn steel: Metallurgy, mechanical properties and warm stamping process. *Mater. Des.* **2016**, *94*, 424–432. [CrossRef]
13. Li, X.; Chang, Y.; Wang, C.; Hu, P.; Dong, H. Comparison of the hot-stamped boron-alloyed steel and the warm-stamped medium-Mn steel on microstructure and mechanical properties. *Mater. Sci. Eng. A* **2017**, *679*, 240–248. [CrossRef]
14. Wang, C.; Li, X.; Han, S. Warm stamping technology of the medium manganese steel. *Steel Res. Int.* **2017**, 1700360. [CrossRef]
15. Li, X.; Chang, Y.; Wang, C.; Han, S.; Ren, D.; Hu, P.; Dong, H. Investigation on Microstructure and Martensitic Transformation mechanism for the warm-stamped third-generation automotive medium-Mn steel. *J. Eng. Mater. Technol.* **2017**, *139*, 041009. [CrossRef]
16. Dong, H.; Cao, W.Q.; Shi, J.; Wang, C.Y.; Wang, M.Q.; Weng, Y.Q. Microstructure and performance control technology of the 3rd generation auto sheet steels. *Iron Steel* **2011**, *46*, 1–11.
17. Chang, Y.; Wang, C.; Zhao, K.; Dong, H.; Yan, J. Introduction to a third-generation automobile steel and its optimal warm-stamping process. *J Manuf. Sci. Eng.* **2016**, *138*, 041010. [CrossRef]
18. Wen, Y.-H.; Zhu, G.-M.; Dai, S.-Y.; Kang, Y.-L. Effect of Ti on microstructure and strengthening behavior in press hardening steels. *J. Cent. South Univ.* **2017**, *24*, 2215–2221. [CrossRef]
19. Lin, L.; Li, B.-S.; Zhu, G.-M.; Kang, Y.-L.; Liu, R.-D. Effect of niobium precipitation behavior on microstructure and hydrogen induced cracking of press hardening steel 22MnB5. *Mater. Sci. Eng. A* **2018**, *721*, 38–46. [CrossRef]
20. Wen, Y.H.; Zhu, G.M.; Hao, L.; Dai, S.Y.; Kang, Y.L. Microstructure and mechanical properties of Nb-Ti micro-alloy hot stamping steels. *Chin. J. Eng.* **2017**, *39*, 859–866.
21. Wen, Y.H. Study of Micro-Alloy and Numerical Simulation Based on 1500 MPa Ultra-High Strength Steels. Master's Thesis, University of Science and Technology Beijing, Beijing, China, 2019; pp. 23–25.
22. Gladman, T. On the theory of the effect of precipitate particles on grain growth in metals. *Proc. R. Soc. Lond. Ser. A Math. Phys. Sci.* **1966**, *294*, 298–309.
23. Gladman, T. Precipitation hardening in metals. *Met. Sci. J.* **1999**, *15*, 30–36. [CrossRef]
24. Lewandowska, M.; Kurzydlowski, K.J. Synergic effects of grain refinement and precipitation strengthening. *J. Mater. Sci.* **2010**, *45*, 4877–4883. [CrossRef]

25. Duan, X.G.; Cai, Q.W.; Wu, H.B. Ti-Mo ferrite matrix micro-alloy steel with nanometer-sized precipitates. *Acta Metall. Sin.* **2011**, *47*, 251–256.
26. Jin, F. Experimental Research on Mechanical Properties and Formality of Medium Manganese Steel. Master's Thesis, Dalian University of Technology, Dalian, China, 2015; pp. 13–15.
27. Yong, Q.L. *Secondary Phases in Steel*; Metallurgical Industry Press: Beijing, China, 2006; pp. 28–64.
28. Tamura, I. *Thermomechanical Processing of High-Strength Low-Alloy Steels*; Butterworth-Heinemann Press: Oxford, UK, 1988; Volume 10, pp. 556–566.
29. Kitahara, H.; Ueji, R.; Tsuji, N.; Minamino, Y. Crystallographic features of lath martensite in low-carbon steel. *Acta Mater.* **2006**, *54*, 1279–1288. [CrossRef]
30. Morito, S.; Yoshida, H.; Maki, T.; Huang, X. Effect of block size on the strength of lath martensite in low carbon steels. *Mater. Sci. Eng. A* **2006**, *438*, 237–240. [CrossRef]
31. Morito, S.; Saito, H.; Ogawa, T.; Furuhara, T.; Maki, T. Effect of Austenite Grain Size on the Morphology and Crystallography of Lath Martensite in Low Carbon Steels. *ISIJ Int.* **2005**, *45*, 91–94. [CrossRef]
32. Sodjit, S.; Uthaisangsuk, V. Microstructure based prediction of strain hardening behavior of dual phase steels. *Mater. Des.* **2012**, *41*, 370–379. [CrossRef]